Chemical Engineering Journal 162 (2010) 217–226

Contents lists available at ScienceDirect

Chemical Engineering Journal

journal homepage: www.elsevier.com/locate/cej

# Modeling of the fluid dynamics and $SO_2$ absorption in a gas–liquid reactor

Luca Marocco*

*Alstom Power Italy, v.le Edison, 50, 20099 Sesto San Giovanni, Milano, Italy*

ARTICLE INFO

*Article history:*
Received 27 October 2009
Received in revised form 12 May 2010
Accepted 15 May 2010

*Keywords:*
CFD
Desulphurisation
Absorption
Euler–Lagrange

ABSTRACT

This paper illustrates a computational fluid dynamic (CFD) model of a counter-current Open Spray Tower desulphurisation reactor and its application in the simulation of a full-scale industrial equipment. The raw flue gas flows upward while a suspension of water and limestone is sprayed downward from different heights. Thereby sulfur dioxide is washed out of the gas.

The two-phase gas–liquid flow inside the equipment has been simulated with an Euler–Lagrange approach using a commercial CFD code, while a model for the $SO_2$ absorption has been developed and implemented in the software through dedicated modules. Physical absorption is modeled using dual-film theory and appropriate empirical and semi-empirical correlations. The aqueous phase chemistry accounts for the instantaneous equilibrium reactions of eight dissolved species into a slurry droplet. The model is used to simulate an industrial plant at different operating conditions. The numerical results are in good agreement with the measured values of pressure drop and sulphur removal efficiency.



## 1. Introduction

Sulfur dioxide removal from flue gases has probably been the subject of more research than any other gas purification operation. Since the vast majority of $SO_2$ emissions are from fossil fuel-fired boilers at power stations, these sources have been widely controlled. Among the different desulphurisation equipments, Open Spray Towers (OST) are the most frequently installed scrubber types for limestone Wet Flue Gas Desulphurisation (WFGD) plants and they cover the major part of the market today.

The process consists in spraying a suspension of water and calcium carbonate ($CaCO_3$) in counter-current to the upward flowing gas. The liquid phase is injected through nozzles, in form of fine droplets, located at different heights. The liquid is then collected in the bottom of the reactor, the so-called reaction tank, and is subsequently pumped again to the spraying levels. The high interface area of the liquid particles and the intimate contact between the two phases promote the mass transfer of $SO_2$ from the gas phase to the liquid phase. Due to its importance, flue gas desulphurisation has been widely studied (Klingspor and Cope [1]) and several mathematical models describing the chemistry of the process are available, e.g. Mehta [2], Olausson et al. [3], Agarwal and Rochelle [4], Brogren and Karlsson [5], Eden and Luckas [6], Kiil et al. [7], Warych and Szymanowski [8]. These previous works do not consider the gas and liquid hydrodynamics inside the absorption tower although there is experimental evidence of the importance of the flow pattern in the desulphurisation process (Nygaard et al. [9]).

Gomez et al. [10] first simulated a full-scale FGD plant applying an Euler–Euler approach for the multiphase flow in the combined packed-and spray tower absorber, while Marocco et al. [11] simulated an OST pilot plant with an Euler–Lagrange approach.

This paper extends the results of the latter work to a full-scale FGD OST. The complex fluid dynamic and chemical processes occurring during the absorption of sulphur dioxide can be properly evaluated with the developed model, which computes the local and global $SO_2$ mass transfer between the phases.

ANSYS-FLUENT 6.3.26, completed with the developed modules for the sulphur dioxide absorption, has been used to simulate a full-scale industrial OST operating at different conditions, i.e. by varying the amount of the injected slurry flow. The numerical results have been compared with the measured data of pressure drop and $SO_2$ removal efficiency.

## 2. Governing equations

The flow in the spray tower is actually a three-phase flow of a gas, liquid and solid phase, the latter being the $CaCO_3$ particles inside the liquid droplets.

Aim of the developed CFD model is to analyze the spray zone, where the main interaction is between the gas and liquid phase. Only this part of the WFGD system is simulated. The liquid–solid interaction is supposed, supported by experimental evidence, to occur mainly in the reaction tank and is therefore neglected in this study (see Fig. 1). The fluid dynamics inside an OST, described as a two-phase flow consisting of a carrier gas

* Tel.: +39 328 2321735.
*E-mail address:* luca.marocco@polimi.it.

1385-8947/$ – see front matter © 2010 Elsevier B.V. All rights reserved.
doi:10.1016/j.cej.2010.05.033

**Nomenclature**

| | |
|---|---|
| $A$ | area ($m^2$) |
| $C_D$ | drag coefficient |
| $D$ | droplet diameter (m) |
| $D_{AB}$ | binary gas diffusion coefficient of $A$ in $B$ ($m^2/s$) |
| $D_{SO_2-H_2O,l}$ | binary liquid diffusion coefficient of $SO_2$ in $H_2O$ ($m^2/s$) |
| $E_{SO_2}$ | enhancement factor of $SO_2$ |
| $F_{i,k}$ | sum of the forces acting at the interface between the phases (N) |
| $g$ | acceleration of gravity |
| $H_{SO_2}$ | Henry's coefficient of $SO_2$ (Pa $m^3$/mol) |
| $k$ | turbulent kinetic energy |
| $k_{SO_2,g}$ | $SO_2$ gas-side mass transfer coefficient |
| $k_l$ | liquid side mass transfer coefficient with chemical reactions (m/s) |
| $k^0_{SO_2,l}$ | $SO_2$ liquid-side mass transfer coefficient without chemical reactions (m/s) |
| $K_X$ | equilibrium constant of reaction $X$ ($mol/m^3$) |
| $K_{SO_2,tot}$ | global $SO_2$ mass transfer coefficient |
| $K_W$ | ionic product of water ($(mol/m^3)^2$) |
| $m_X$ | concentration of species $X$ in liquid bulk ($mol/m^3$) |
| $\dot{m}$ | mass flow rate |
| $M$ | molecular mass |
| $N_{SO_2}$ | $SO_2$ molar flux |
| $p$ | gas pressure |
| $P_{SO_2}$ | partial pressure of $SO_2$ in gas bulk |
| $\Re$ | universal gas constant |
| $Re_r$ | relative Reynolds number |
| $S_{A,mass}$ | gas phase species source term ($kg/m^3$ s) |
| $S_{k,mass}$ | droplet mass source (kg/s) |
| $S_{k,mom}$ | droplet momentum source (N) |
| $S_{mass}$ | gas phase mass source ($kg/m^3$ s) |
| $S_{mom}$ | gas phase momentum source ($N/m^3$) |
| Sc | Schmidt number |
| Sh | Sherwood number |
| $t$ | time |
| $T$ | temperature |
| TC | total carbon concentration in slurry ($mol/m^3$) |
| TS | total sulphur concentration in slurry ($mol/m^3$) |
| **u** | gas velocity vector |
| **v** | droplet velocity vector |
| $V$ | averaging/element volume ($m^3$) |
| **x** | position vector |

*Greek symbols*

| | |
|---|---|
| $\gamma_\pm$ | mean activity coefficient |
| $\varepsilon$ | turbulent kinetic energy dissipation |
| $\eta_{SO_2}$ | Sulphur dioxide removal efficiency |
| $\mu$ | gas phase dynamic viscosity |
| $\mu_{H_2O}$ | water viscosity |
| $\rho$ | continuous phase density |
| $\tau$ | Continuous phase stress tensor |
| $\tau^R$ | Reynolds stress tensor |
| $\omega$ | mass fraction, kg/kg |

*Subscripts*

| | |
|---|---|
| $A$ | generic component $A$ |
| d | droplet |
| g | gas |
| $i$ | $i$-th element |
| $k$ | $k$-th droplet |
| l | liquid |
| (aq) | aqueous phase |
| (g) | gas phase |
| (s) | solid phase |

and a large number of dispersed liquid droplets, has been simulated with an Euler–Lagrange approach (Lapin and Lübbert [12]). The continuous gas phase is modeled in an Eulerian framework, while the dispersed liquid phase with a Lagrangian approach by tracking a large number of particles through the computational domain. The Euler–Lagrange approach has been preferred over the Euler–Euler approach because for a dispersed flow, like the one in Open Spray Towers, particle-level phenomena can be modeled rigorously, thus allowing to accommodate complicated forms of interphase physical processes. Furthermore, droplet size distribution and droplet–wall interaction, both aspects very important in spraying equipment, can be easily taken into account.

The final form of the gas- and dispersed phase conservation equations is summarized in Table 1.

### 2.1. Carrier phase

According to Marocco et al. [11] the liquid volume fraction inside an OST is everywhere lower than 5–8% except in a small portion of the computational domain very close to the spray nozzles. The continuous gas phase can then be regarded as a single-phase, neglecting the influence of the small volume fraction occupied by the dispersed liquid phase. Particle–particle interactions are also negligible. Moreover the flue gas temperature is almost immediately cooled down to its saturation value after the gas enters the tower. Therefore the present work considers the flue gas at scrubber inlet already saturated with water. The temperature of both phases is then the same all through the computational domain and equal to the saturation temperature. This allows to neglect the energy equation for both phases allowing a considerable computational time saving for simulations with a very high number of elements.

Assuming droplets of spherical shape and according to Crowe et al. [13] and Marocco et al. [11] the conservation equations of the continuous phase assume the same formulation as the conservation equations of a single-phase flow with the addition of source terms, which represent mass ($S_{mass}$ and $S_{A,mass}$) and momentum ($S_{mom}$)

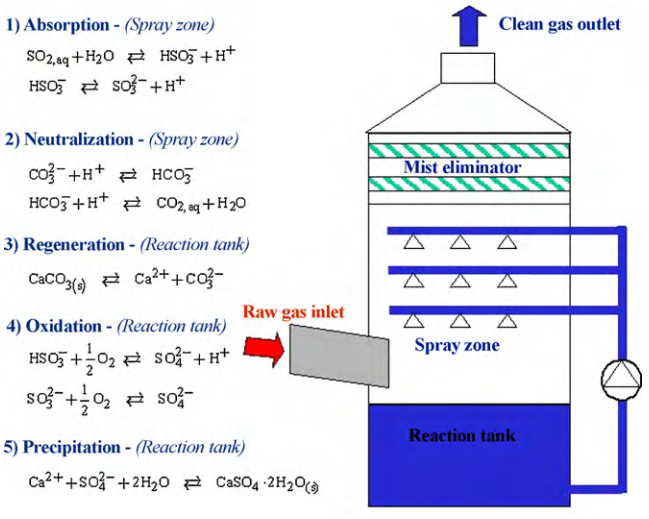


**Fig. 1.** Schematic picture of a WFGD scrubber along with the chemical reactions occurring inside of it.

**Table 1**
Conservation equations for the gas and dispersed phase. $f = C_d Re_r/24$ is the drag factor, i.e. the ratio of the drag coefficient to Stokes drag, $M_{SO_2}$ is $SO_2$ molecular weight.

| | Gas phase conservation equations | Source terms | Liquid phase conservation equations |
|---|---|---|---|
| Continuity | $\frac{\partial}{\partial t}\rho + \nabla\cdot(\rho u) = 0$ | $S_{mass} = 0$ | Same as species |
| Momentum | $\frac{\partial}{\partial t}\rho\mathbf{u} + \nabla\cdot(\rho\mathbf{u}\otimes\mathbf{u}) = -\nabla p + \nabla\cdot(\tau + \tau^R) + \rho\mathbf{g} + S_{mom}$ | $S_{mom} = -\frac{1}{V}\sum_k \mathbf{v}_k \dot{m}_{SO_2,k} - \frac{3\pi\mu}{V}\sum_k D_k f_k(\mathbf{u}-\mathbf{v}_k)$ | $m_d \frac{d\mathbf{v}}{dt} = 3\pi\mu D f(\mathbf{u}-\mathbf{v})$ |
| Species | $\frac{\partial}{\partial t}(\rho\omega_{SO_2}) + \nabla\cdot(\rho\omega_{SO_2}\mathbf{u}) = \nabla\cdot(\rho D_{SO_2-air}\nabla\omega_{SO_2}) + S_{SO_2,mass}$ | $S_{SO_2,mass} = -\frac{1}{V}\sum_k \dot{m}_{SO_2,k}$ | $\frac{dm_d}{dt} = M_{SO_2} A_d K_{SO_2,tot}(P_{SO_2} - H_{SO_2} m_{SO_2})$ |

coupling between the phases:

$$\frac{\partial}{\partial t}\rho + \nabla\cdot(\rho\mathbf{u}) = S_{mass} \tag{1}$$

$$\frac{\partial}{\partial t}(\rho\boldsymbol{u}) + \nabla\cdot(\rho\boldsymbol{u}\otimes\boldsymbol{u}) = -\nabla p + \nabla\cdot(\boldsymbol{\tau} + \boldsymbol{\tau}^R) + \rho\boldsymbol{g} + S_{mom} \tag{2}$$

$$\frac{\partial}{\partial t}(\rho\omega_A) + \nabla\cdot(\rho\omega_A\boldsymbol{u}) = \nabla\cdot(\rho D_{AB}\nabla\omega_A) + S_{A,mass} \tag{3}$$

Turbulence energy and dissipation rate can be affected by the presence of dispersed particles. This effect is known as turbulence modulation. Source terms should be added in the turbulence equations to account for it. Anyway, there is experimental evidence that modulation is weak if the particle concentration is very low, as in this work. Therefore the $k$–$\varepsilon$ realizable model has been used in its formulation for single-phase flows (Shih et al. [14]) to simulate turbulence in the continuous phase flow and the Reynolds stress tensor has been related to the mean properties of the flow following Boussinesq assumption. The physical presence of the particles in the flow creates velocity disturbances which will contribute to the Reynolds stress also in the absence of mean velocity gradients. Therefore the Boussinesq assumption is not appropriate and a better approach may be to use the Reynolds Stress Model which circumvents the need for it. Anyway, the boundary conditions for this model are typically unknown for the case of WFGD systems.

The source terms are calculated by volume averaging the contributions from all the individual droplets within the cell volume (Marocco and Inzoli [11]).

$$S_{mass} = -\frac{1}{V}\sum_{A,k}\dot{m}_{A,k} \tag{4}$$

$$S_{mom} = -\frac{1}{V}\sum_{A,k} v_k \dot{m}_{A,k} - \frac{1}{V}\sum_{i,k}\boldsymbol{F}_{i,k} \tag{5}$$

$$S_{A,mass} = -\frac{1}{V}\sum_{k}\dot{m}_{A,k} \tag{6}$$

After evaluation of these source terms, the gas phase conservation equations need to be solved again (*two-way coupling*). The resulting flow and concentration fields are then used to calculate updated source terms and so on until convergence.

### 2.2. Dispersed phase

Once the gas velocity field is known, the particles trajectories can be computed. The dispersed liquid phase is calculated with a Lagrangian approach by tracking a large number of particles, called *parcels*, through the computational domain. It is assumed that the parcel of particles moves through the computational domain with the same properties (velocity, density, etc.) as a single physical particle. A parcel is commonly identified as a discrete element.

The continuity and momentum equations for a single non-rotating parcel take the following form (the subscript d indicates that the quantity is referred to a droplet):

$$\frac{d\boldsymbol{x}}{dt} = v \tag{7}$$

$$\frac{dm_d}{dt} = S_{k,mass} \tag{8}$$

$$m_d\frac{dv}{dt} = S_{k,mom} + m_d\boldsymbol{g} \tag{9}$$

Starting from injection conditions specified for each nozzle, these ordinary differential equations are solved by stepwise integration over discrete time steps, using the continuous phase flow properties at the current droplet position.

The evaluation of the particle's source terms in Eqs. (8) and (9) for a spherical non-rotating droplet, allows the determination of the source terms in the gas phase flow equations.

#### 2.2.1. Momentum source term

According to Eq. (5), momentum is exchanged between phases through mass transfer and interphase forces.

The determination of the momentum source term associated with mass exchange follows from the calculation of mass transfer between phases.

The motion of an *isolated* particle inside the computational domain can be described through the Basset–Boussinesq–Oseen (BBO) equation. The momentum source term in Eq. (9) is the sum of the forces acting at the interface of a particle, $\mathbf{F}_{i,k}$.

According to Crowe et al. [13], Eq. (9) can be written as:

$$m_d\frac{dv}{dt} = \frac{1}{2}\rho C_D|\boldsymbol{u}-\mathbf{v}|(\boldsymbol{u}-\mathbf{v})A_d + m_d\boldsymbol{g} + O\left(\frac{\rho}{\rho_d}\right) \tag{10}$$

Therefore, in gas–liquid flows where the above density ratio is low, the only two forces that significantly contribute to the particle's linear momentum variation are the steady-state drag force and the gravity force.

The drag coefficient is evaluated through the Morsi and Alexander [15] correlation, that adjusts the value of $C_D$ for a spherical particle over a wide range of relative Reynolds numbers, $Re_r = \rho D|\boldsymbol{u}-\mathbf{v}|/\mu$:

$$C_D = a_1 + \frac{a_2}{Re_r} + \frac{a_3}{Re_r^2} \tag{11}$$

In the above equation, the coefficients $a_i$ are functions of $Re_r$.

#### 2.2.2. Mass source terms

The present study considers only the absorption of $SO_2$ from the flue gas mixture into the slurry droplets. The source term in Eq. (8) can then be written as:

$$S_{k,mass} = S_{k,SO_2} = \dot{m}_{SO_2} \tag{12}$$

The mass flow rate of $SO_2$ is very low compared to the total flue gas mass flow rate. It is then assumed that its absorption does not impact the gas phase continuity Eq. (1): $S_{mass} = 0$.

Mass transfer of sulphur dioxide involves both gas side and liquid side mass transfer resistances. For low dissolved gas con-

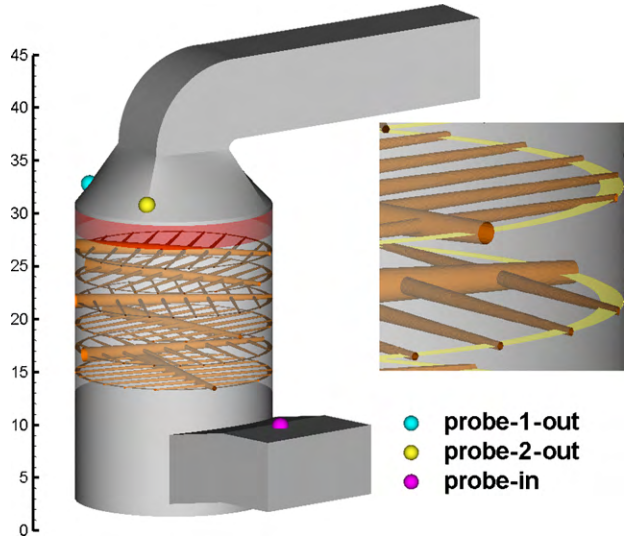


**Fig. 2.** Computational domain and location of the measuring probes. The highlighted surface below the outlet cone indicates the mist eliminator.

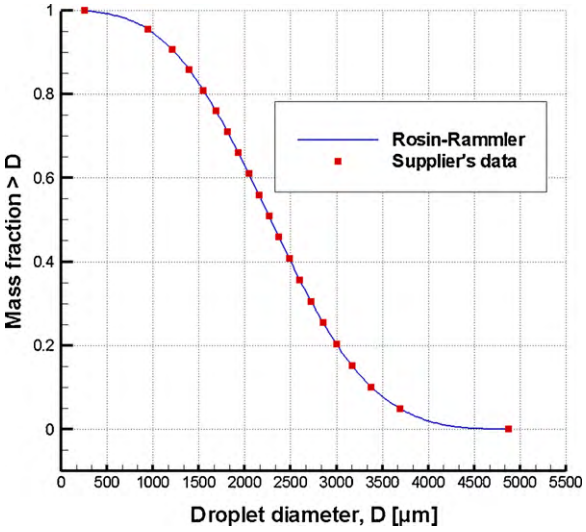


**Fig. 4.** Droplets size distribution with Rosin–Rammler interpolation.

centrations Henry's law can be applied and the molar rate of $SO_2$ mass transfer assumes the form:

$$N_{SO_2} = K_{SO_2,tot}(P_{SO_2} - H_{SO_2} m_{SO_2}) = \frac{\dot{m}_{A,k}}{M_{SO_2}} \quad (13)$$

The global $SO_2$ mass transfer coefficient is expressed as:

$$\frac{1}{K_{SO_2,tot}} = \frac{1}{k_{SO_2,g}} + \frac{H_{SO_2}}{E_{SO_2} k^0_{SO_2,l}} \quad (14)$$

The present work considers conditions far away from the nozzles where the liquid side mass transfer coefficient in the absence of chemical reactions can be expressed by (Perry and Green [16]):

$$k^0_{SO_2,l} = 10\frac{D_{SO_2-H_2O,l}}{D} \quad (15)$$

The value of the binary liquid diffusion coefficient of $SO_2$ in aqueous solution, $D_{SO_2-H_2O,l}$, at 25 °C (Perry and Green [16]) is extrapolated to the value corresponding to the droplet's temperature, considered the same as the gas saturation temperature, using the Stokes–Einstein equation:

$$\frac{D_{SO_2-H_2O,l}\mu_{H_2O}}{T_d} = \text{const} \quad (16)$$

The enhancement factor, $E_{SO_2}$, accounts for a higher driving force in the liquid film compared to an absorption without chemical reactions, which are here supposed to occur in the liquid bulk only. The different empirical and semi-empirical algebraic correlations listed in literature for the calculation of $E_{SO_2}$ are not accurate and therefore it is not worth using them, while more sophisticated models allows to evaluate $E_{SO_2}$ at every droplet position by knowing the interfacial concentrations of $HSO_3^-$, $SO_3^{2-}$ and $SO_2$, which are determined by a balance on local charge and appropriate boundary conditions (Kiil et al. [7]).

According to Brogren and Karlsson [5], the enhancement factor is a function of droplet pH, partial pressure of $SO_2$ in the gas phase and the ratio between $k^0_l$ and $k_g$. The enhancement factor has its highest values at the top of the absorber, where the partial pressure of $SO_2$ is low and the liquid pH is high. The spray tower operates with high enhancement factors (>25) only very close to the nozzles, while the major part of it operates with values in the range of 5–15. The constant value of 10 used in the present work is only an estimation, even though reasonable, and can be interpreted as an adjustable parameter to match the experimental values. Anyway, the more realistic approach of calculating it at every droplet position should be adopted and is presently under development for an upgraded version of the present model.

$H_{SO_2}$ has been evaluated at the saturation temperature using the correlation proposed by Maurer [17]:

$$\ln H_{SO_2} = \frac{A}{T_d} + B \ln T_d + CT_d + D \quad (17)$$

where $A$, $B$, $C$ and $D$ are species dependent coefficients.

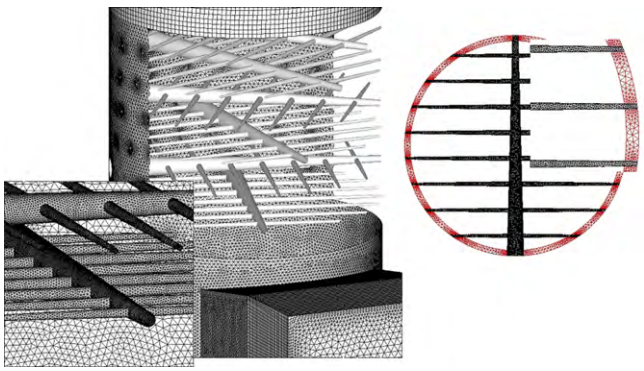

**Fig. 3.** Geometry discretization with finite volumes. Spray zone: tetrahedral cell; outlet cone and duct: hexahedral cells.

**Table 2**
Finite volumes and injections data.

| | |
|---|---|
| Finite volumes elements | |
| Number of control volume cells | 7,650,000 |
| Spray zone up to cone inlet | Tetrahedral |
| Cone and outlet duct | Hexahedral |
| Injections | |
| Number of injection points/nozzle | 40 |
| Number of diameter/injection point | 10 |
| Number of injected parcels/nozzle | 400 |
| Total number of injected parcels/injection | 500,000 |

The gas side mass transfer coefficient, $k_{SO_2,g}$, is evaluated with the modified Ranz–Marshall equation [13]:

$$\mathrm{Sh} = \frac{k_{SO_2,g} D \Re T}{D_{SO_2-air,g}} = 2 + 0.69 Re_r^{0.5} Sc^{0.33} \quad (18)$$

where $T$ is the flue gas temperature.

The molecular diffusion coefficient of $SO_2$ in the flue gas, $D_{SO_2-air,g}$, has been considered equal to the diffusivity of $SO_2$ in air and has been calculated with the Füller–Schettler–Giddings equation (Perry and Green [16]).

The partial pressure of $SO_2$ in the gas bulk is known from the solution of the corresponding gas phase species equation, while a dedicated chemical model has been developed for the evaluation of the dissolved sulphur dioxide concentration in the liquid bulk.

## 3. Aqueous phase chemistry

In a wet limestone scrubbing system, a complex series of kinetic and equilibrium controlled reactions occur in the gas, liquid and solid phases. They may be stated in an overall expression as:

$$SO_{2(g)} + CaCO_{3(s)} + \frac{1}{2}O_{2(g)} + 2H_2O_{(aq)} \rightleftarrows CaSO_4 \cdot 2H_2O_{(s)} + CO_{2(g)} \quad (19)$$

This reaction can be divided in mainly five different steps, all of which occur simultaneously in the scrubber: absorption, neutralization, regeneration, oxidation and precipitation. The developed chemical model considers only the reactions occurring in the spray zone, where the gas–liquid flow is analyzed. Therefore, regeneration, oxidation and precipitation processes are not considered further here because they mainly occur in the reaction tank, as illustrated in Fig. 1.

It is experimentally recognized that the absorption and neutralization reactions can be assumed to be at equilibrium. Together with water dissociation, with a mass balance for the sulphur species, a mass balance for the carbon species and electroneutrality, they form a system of eight non-linear algebraic equations in the eight unknown dissolved species concentrations $SO_{2aq}$, $CO_{2aq}$, $H^+$, $OH^-$, $HSO_3^-$, $SO_3^{2-}$, $HCO_3^-$, $CO_3^{2}$, defining the droplet's liquid phase composition at each trajectory calculation step.

$$\begin{aligned}
&K_{H_2O} = (\gamma_\pm)^2 m_{H^+} m_{OH^-} \\
&K_{SO_{2,aq}} = (\gamma_\pm)^2 \frac{m_{HSO_3^-} m_{H^+}}{m_{SO_{2,aq}}} \\
&K_{HSO_3^-} = \gamma_\pm \frac{m_{SO_3^{2-}} m_{H^+}}{m_{HSO_3^-}} \\
&K_{CO_{2,aq}} = (\gamma_\pm)^2 \frac{m_{HCO_3^-} m_{H^+}}{m_{CO_{2,aq}}} \\
&K_{HCO_3^-} = \gamma_\pm \frac{m_{CO_3^{2-}} m_{H^+}}{m_{HCO_3^-}} \\
&TC = m_{CO_{2,aq}} + m_{HCO_3^-} + m_{CO_3^{2-}} \\
&TS = m_{SO_{2,aq}} + m_{HSO_3^-} + m_{SO_3^{2-}} \\
&2m_{Ca^{2+}} - m_{Cl^-} + m_{H^+} - m_{OH^-} - m_{HCO_3^-} - 2m_{CO_3^{2-}} - m_{HSO_3^-} \\
&-2m_{SO_3^{2-}} = 0
\end{aligned} \quad (20)$$

The equilibrium constants of the reactions are evaluated at the droplets' temperature, equal to the gas saturation temperature, with the following correlation:

$$\ln K_i = \frac{A_i}{T} + B_i \ \ln T + C_i T + D_i \quad (21)$$

The species dependent parameters, $A$, $B$, $C$ and $D$, are taken from the work of Maurer [17] with the exception of the calcite solubility, $K_{CaCO_3}$, which derives from the work of Gage and Rochelle [18].

The concentration of calcium ions and chloride ions is predominant in the aqueous phase. Therefore, the multicomponent solution is assumed to be a single strong electrolyte solution of $CaCl_2$ and the modified form of the Debye–Hückel equation, proposed by Bromley [19], is used to calculate the mean activity coefficient.

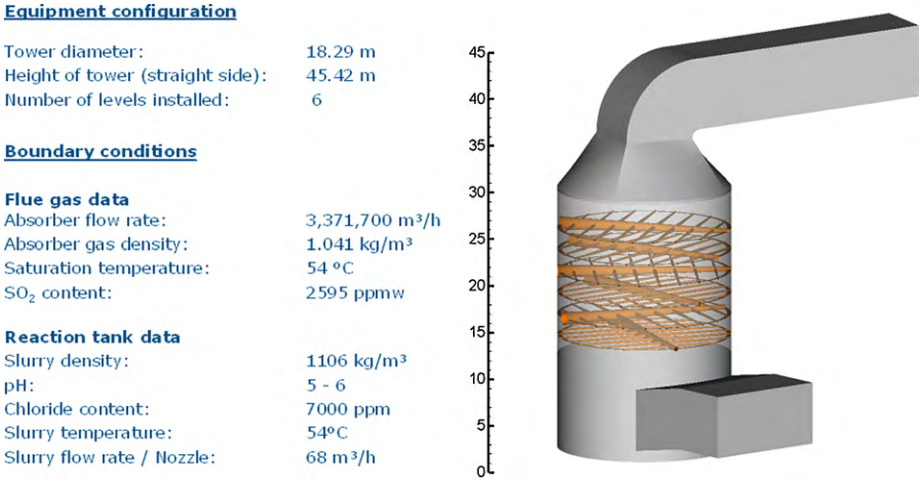


**Fig. 5.** Main geometrical and operating data of the simulated OST.

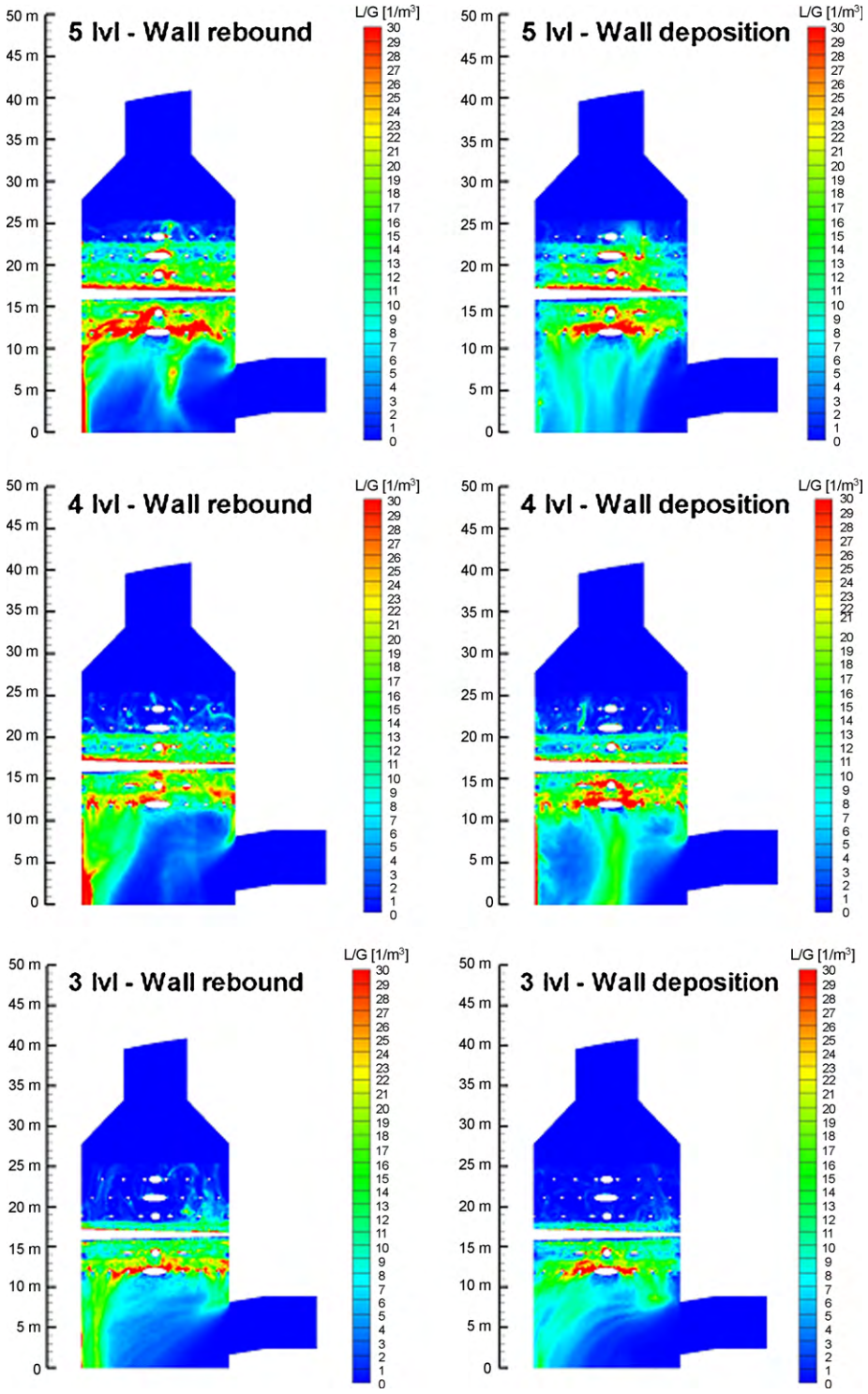


**Fig. 6.** L/G distribution on a plane perpendicular to gas entrance [l/m$^3$].

The systems of Eq. (20) can be written as:

$$2m_{Ca^{2+}} - m_{Cl^-} - \frac{K_{H_2O}}{m_{OH^-}} + \\ -TS\frac{(K_{SO_{2,aq}}/m_{H^+}) + 2(K_{SO_{2,aq}}K_{HSO_3^-}/(m_{H^+})^2)}{1 + (K_{SO_{2,aq}}/m_{H^+}) + (K_{SO_{2,aq}}K_{HSO_3^-}/(m_{H^+})^2)} \\ -TC\frac{(K_{CO_{2,aq}}/m_{H^+}) + 2(K_{CO_{2,aq}}K_{HCO_3^-}/(m_{H^+})^2)}{1 + (K_{CO_{2,aq}}/m_{H^+}) + (K_{CO_{2,aq}}K_{HCO_3^-}/(m_{H^+})^2)} = 0 \quad (22)$$

where TC and TS are expressed as:

$$TC = m_{CO_{2,aq}}\left(1 + \frac{K_{CO_{2,aq}}}{m_{H^+}} + \frac{K_{CO_{2,aq}}K_{HCO_3^-}}{(m_{H^+})^2}\right) \quad (23)$$

$$TS = m_{SO_{2,aq}}\left(1 + \frac{K_{SO_{2,aq}}}{m_{H^+}} + \frac{K_{SO_{2,aq}}K_{HSO_3^-}}{(m_{H^+})^2}\right) \quad (24)$$

Given TC, TS, $m_{Ca^{2+}}$ and $m_{Cl^-}$ Eq. (22) is solved at every droplet position for $m_{H^+}$ with a global Newton method. $m_{SO_{2,aq}}$ is then cal-

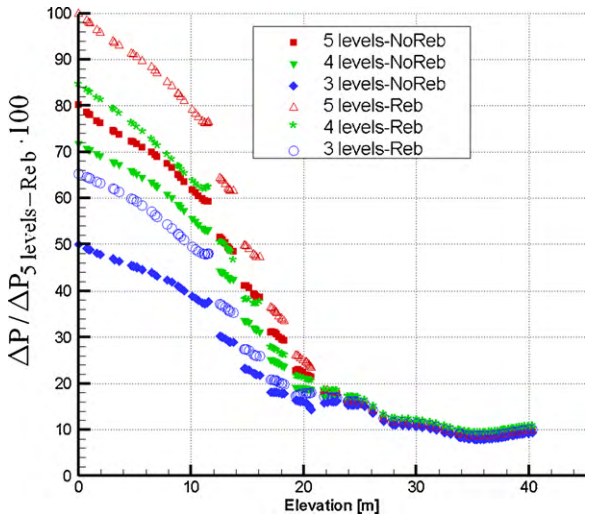


**Fig. 7.** Pressure plot on the centreline of the scrubber; the discontinuities occur when crossing a spray bank.

culated through Eq. (24) and is used for the evaluation of the $SO_2$ mass transfer, Eq. (13), at the next droplet position.

The chloride concentration is a given constant that depends on process and economical considerations (Marocco [20]). At each droplet position inside the computational domain, TS is updated using Eq. (13). Because limestone dissolution and desorption of $CO_2$ into the gas phase are both neglected in the spray zone, $m_{Ca^{2+}}$ and TC in a falling droplet are supposed to remain unchanged. (Desorption of $CO_2$ in the flue gas would also contribute to the absorption of $SO_2$ by increasing the alkalinity of the solution. Anyway, $CO_2$ desorption in the spray zone has been considered small with respect to the same occurring in the reaction tank, where the limestone dissolution contributes to increase the dissolved $CO_2$ and therefore the driving force for mass transfer. A revised model accounting for $CO_2$ desorption in the spray zone is currently under development.) Their evaluation at the injection of a droplet into the computational domain requires the solution of the following auxiliary system of chemical reactions (in the four unknown dissolved species $CO_{2aq}$, $HCO_3^-$, $CO_3^{2-}$, $Ca^{2+}$) occurring in the reaction tank.

$$\begin{aligned} K_{CaCO_3} &= (\gamma_\pm)^2 m_{Ca^{2+}} m_{CO_3^{2-}} \\ K_{CO_{2,aq}} &= (\gamma_\pm)^2 \frac{m_{HCO_3^-} m_{H^+}}{m_{CO_{2,aq}}} \\ K_{HCO_3^-} &= (\gamma_\pm) \frac{m_{CO_3^{2-}} m_{H^+}}{m_{HCO_3^-}} \\ 2m_{Ca^{2+}} + m_{H^+} - m_{Cl^-} - m_{OH^-} - m_{HCO_3^-} - 2m_{CO_3^{2-}} &= 0 \end{aligned} \tag{25}$$

The pH in the reaction tank is buffered to a constant value, and thus also $m_{H^+}$ and $m_{OH^-}$, that depends on process and economical considerations (Marocco [20]).

The above system of equations reduces to a second-order non-linear equation in $m_{CO_{2,aq}}$. Its solution allows then the determination of TC and $m_{Ca^{2+}}$.

## 4. Liquid–wall interaction

A considerable amount of the injected slurry impacts on the scrubber internals, like walls and spray banks. Therefore it is necessary to handle the droplets trajectory modification due to this interaction. Two different events can occur when a parcel hits a wall: splashing and deposition. Splashing occurs when the droplet impact energy exceeds an upper limit, which depends on the surface characteristics, i.e. roughness, curvature, wettability and film thickness. Experimental and numerical investigations (Weiss and Wieltsch [21]; Marocco and Inzoli [11]) have shown that the pressure drops in a pilot plant were best predicted by an ideal reflection model, i.e. by the rebound of every droplet impacting onto the walls. In order to evaluate the influence of the liquid–wall interaction on the pressure drop and on the removal efficiency in a huge scrubber, each simulation has been performed both with a complete rebound of a droplet hitting an internal surface and with a total deposition on it. Moreover it has been assumed that at each impact the tangential component of the droplet's rebound velocity remains unchanged while the normal component is halved.

## 5. Computational domain and boundary conditions

The simulated full-scale OST is located in USA. Fig. 2 illustrates the computational domain, together with the location of the measuring probes. Gas guiding means, called Wall Rings (patent by ABB FLAKT [22]), are installed between each level to prevent bypass of partially scrubbed flue gas at the perimeter walls of the absorber, improving gas-slurry contact and thus increasing sulphur dioxide removal (Brogren et al. [23], Hofelsauer et al. [24]). The bottom plane of the reactor represents the free liquid surface of the slurry collected in the reaction tank. The performance tests, in June 2007, highlighted a sulphur dioxide removal efficiency and pressure drops much higher than estimated in the design phase. The 0D model, based on empirical correlations, failed in the prediction of the equipment performances. An extensive measurement campaign has been done by varying the scrubber operating conditions, in terms of number of spray banks in operation and flue gas flow rate, in order to understand the reasons of this discrepancy. The present study simulates the gas and liquid hydrodynamics inside the scrubber together with the chemisorption of $SO_2$. Three different operating conditions have been simulated, i.e. with five, four and three spray levels in operation.

As previously discussed each simulation has been performed with a complete rebound of a droplet hitting an internal surface and with a total deposition on it.

Particular attention has been dedicated to the discretization of the computational domain, Fig. 3, because of the different characteristic lengths of the geometrical elements. The nozzles are not geometrically modeled but they are treated as slurry injection points. This simplification is justified by the negligible impact of their dimensions on the scrubber hydrodynamics compared to the other geometrical entities. Their presence would only significantly complicate the discretization of the domain. Locations, type and operating parameters are specified for each nozzle. The liquid emerges from the nozzle's orifice as a thinning unstable sheet that further away from the discharge surface breaks into ligaments and finally droplets. The modeling of this disintegration process requires a huge computational effort. Therefore, when dealing with many injections and big computational domains, it is necessary to simplify the droplets generation process. In this study the liquid flow ejected from the nozzles is simulated as an ensemble of spherical droplets. The droplet size distribution has been reproduced by fitting the supplier's data through the Rosin–Rammler expression, Fig. 4. The number of injected discrete elements (parcels) has been gradually increased in order to obtain a numerical solution independent from it. Table 2 summarizes the mesh and injections characteristics.

As shown in Fig. 2 a mist elimination system is installed before the absorber's outlet cone in order to collect the liquid droplets, thus avoiding to plug the gas path and to increase the particulate emissions at the stack. The discretization of its geometry would require a very high number of small control volumes. Therefore, the mist eliminator is modeled as a porous block with a specified pressure drop according to the manufacturer's specifications. In the

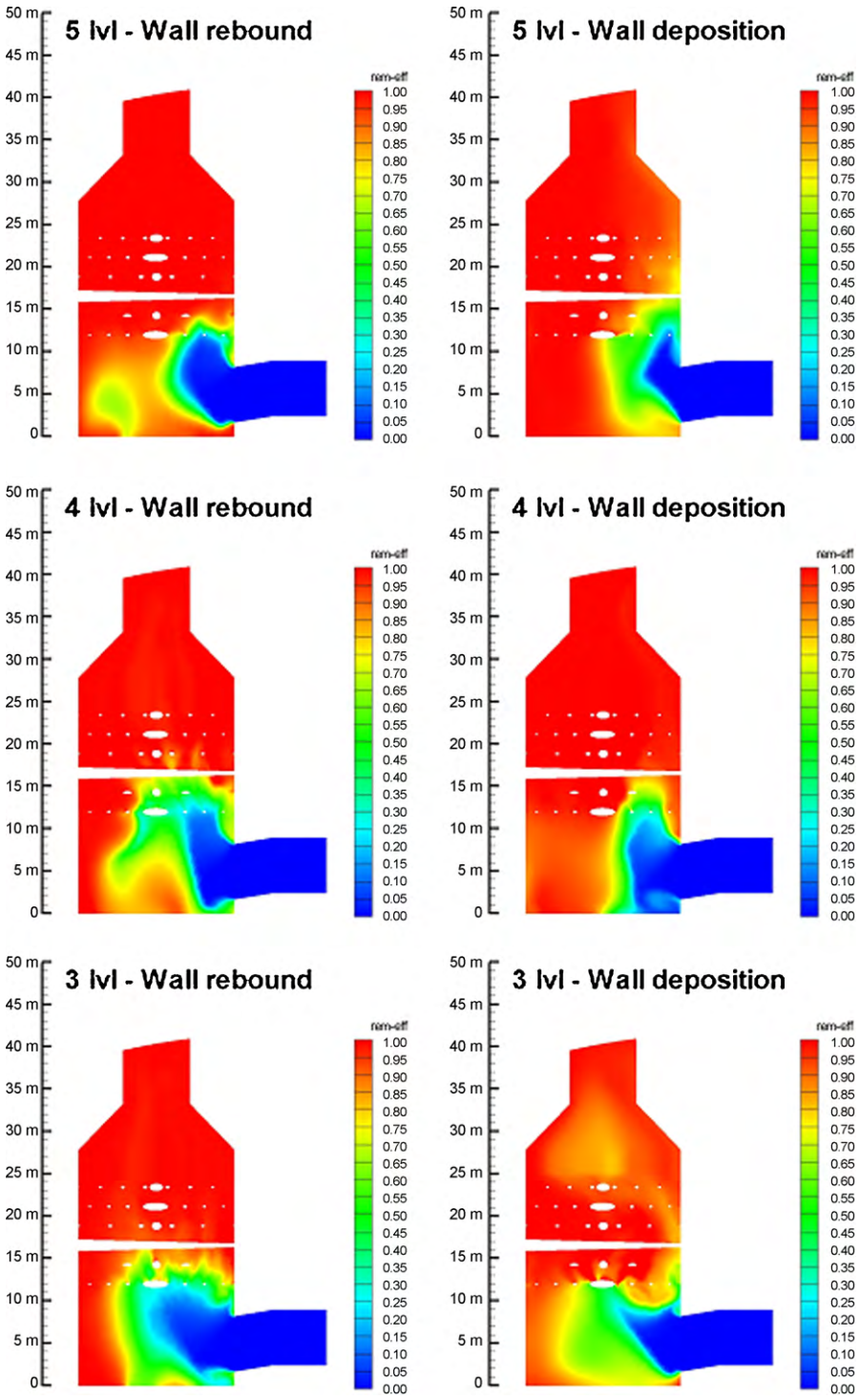


**Fig. 8.** $SO_2$ distribution on a plane perpendicular to gas entrance.

simulations the mist eliminator is considered as a perfect droplets collector. After the mist eliminator no liquid phase is dispersed into the flue gas.

### 5.1. Flue gas and slurry properties

The gas phase is considered a Newtonian mixture of sulphur dioxide and inert air and it obeys the perfect gas law. The flue gas density and viscosity are constant all through the computational domain, while the $SO_2$ mass diffusivity in air is calculated with the Füller–Schettler–Giddings correlation.

The density and viscosity of the slurry droplets remain unchanged all through the computational domain.

The main geometrical dimensions of the simulated OST, together with the flue gas and slurry data, are summarized in Fig. 5.

### 5.2. CFD simulation and results

A steady-state flow has been considered for all the simulations performed and the Simple algorithm has been used for the pressure velocity coupling. To improve the convergence behavior, the flow of the flue gas phase alone has been first computed. Upon

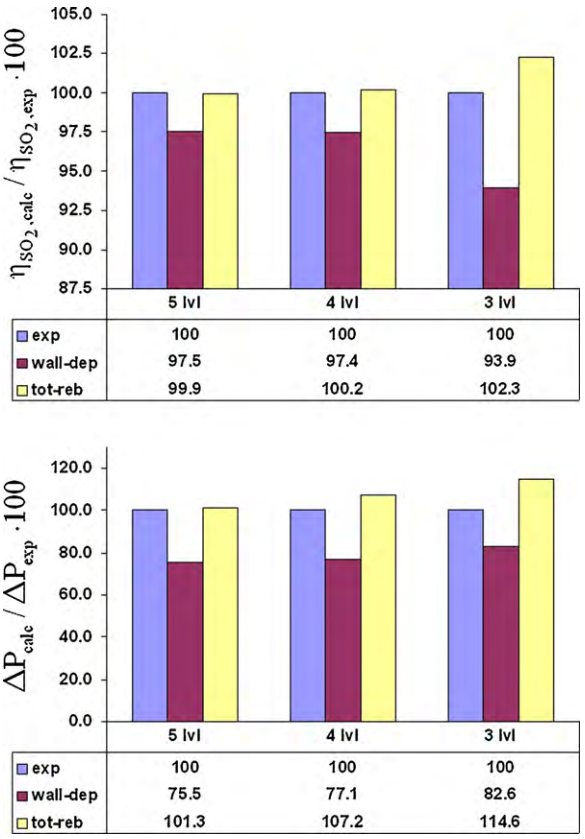


**Fig. 9.** Comparison between measured and calculated pressure drop and $SO_2$ removal efficiency.

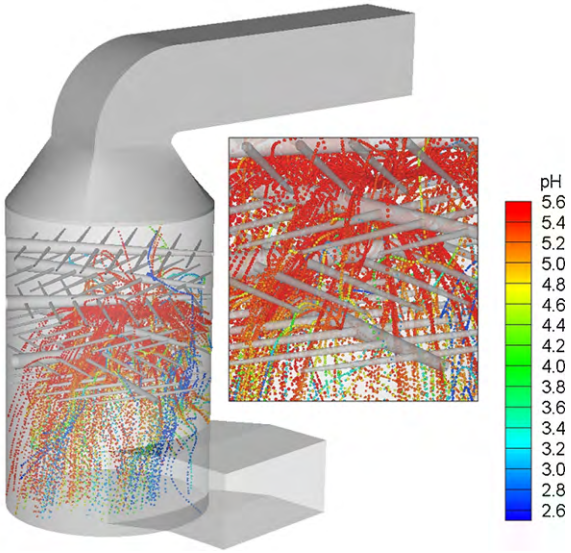


**Fig. 10.** Particle trajectories from a dual flow nozzle located on the 3rd spray bank, colored by pH; ideal reflection on the walls.

obtaining the solution for the primary phase, the injection of the dispersed liquid phase, and thus the source terms for continuous phase, has been turned on. The problem presents a high discrete phase mass loading, implying high source terms in the momentum equation. Therefore a proper management of the under-relaxation factor for the momentum source terms is required. This has been kept very low (0.001) at the beginning of the simulation and has been progressively increased (up to 0.1) in order to keep the numerical solution stable and to speed up the convergence. Upon reaching a stable fluiddynamic solution of the coupled gas–liquid flow, the $SO_2$ absorption (species equation) and the chemical model have been activated and solved separately from the gas momentum and continuity equations. This is justified by the small $SO_2$ flow rate that does not influence the velocity field inside the reactor. The numerical simulation has been run in parallel on a cluster of 8 processors Xeon with 4 GB RAM each and every simulation took approximately 120 h (35,000 iterations of the continuous phase) to get a converged solution.

Fig. 6 shows the L/G distribution, i.e. the local ratio between the liquid and the gas flow occupying the cell volume, on a section perpendicular to the raw gas entrance for all the three operating conditions analyzed. The simulations with and without droplets' rebounds show for each case pronounced differences, especially close to the walls. This justifies the pressure drop difference between the two solutions, as shown in Fig. 7. The two calculated values of pressure drop ("NoReb" and "Reb") define then the upper and lower limit for the specific case. Of course the L/G distribution and the pressure drop vary by varying the number of operating spray banks.

The $SO_2$ distribution field on a section perpendicular to the raw gas entrance is shown in Fig. 8, where the sulphur dioxide removal efficiency is defined as $\eta_{SO_2} = 1 - \omega_{SO_2}(x)/\omega_{SO_{2,in}}$.

Despite the differences in the L/G distribution, the $SO_2$ distribution is quite similar for the cases with five and four operating levels, with both boundary conditions on the walls. Conversely, the two solutions (wall rebound, wall deposition) with three operating levels are rather different. The case with liquid deposition on the walls shows an inhomogeneous distribution of $SO_2$ and values of removal efficiency much lower than the case with ideal reflection of the impacting droplets. The reason is that a substantial fraction of the injected slurry flow rate is lost on the walls, contributing only partially to sulphur dioxide removal. This effect is strongly reduced for the cases with five and four operating levels with wall deposition because the slurry flow rate is so high that the liquid fraction deposited on the walls does not influence the resulting $SO_2$ removal efficiency.

The parameters that have been measured at the positions illustrated in Fig. 2 are static pressure and sulphur dioxide concentration. Fig. 9 illustrates the comparison between numerical results, evaluated at the probes' positions, and experimental data.

The numerical results from the CFD simulations are in very good agreement with the measured values of $SO_2$ removal efficiency, while larger differences appear in the pressure drops. As already found by Marocco et al. [11] and Weiss et al. [21], the pressure drops with the ideal reflection model only slightly over-estimate the experimental values while the calculated pressure drop with total wall deposition under-estimate them. This stems from the physical observation that a rebounding droplet can divide in several droplets (splashing event) that increase the momentum source terms compared to a single rebounding drop. Even though not every impacting droplet rebounds, the ideal reflection model reproduces the higher pressure drops generated from the increased number of secondary splashed droplets, giving more realistic results.

It must be underlined that the numerical values of $SO_2$ removal efficiency are in very good agreement with measurement and they do not vary significantly for the cases with five and four spray levels in operation. The wall boundary effect is buffered by the very high amount of slurry injected, which makes the chemical solution almost independent from the droplet–wall interaction model. At lower liquid flow rates the wall effect is more evident. The simulation with three operating levels shows a big difference between the removal efficiency with and without wall rebounds. The reasons for this have been previously discussed.

Fig. 10 shows the trajectories, colored by pH, of the particles injected from a nozzle located on the third spray bank. It is remarkable that the pH does not vary when the droplets are close to the nozzles. When reaching the third level, the flue gas is already scrubbed from $SO_2$. There is neither further $SO_2$ absorption nor subsequent dissociation of the dissolved $SO_2$, which would produce hydrogen ions and thus lower the pH. The scrubber could therefore operate with less active spray levels achieving the same removal efficiency.

## 6. Conclusions

Today, the design of Open Spray Towers (OST) is essentially based on empirical and/or semi-empirical correlations that are only valid for a limited range of the design parameters, while the optimization of the fluid dynamics and chemistry of these equipments is necessary to comply with the stringent $SO_2$ emission requirements.

A model to calculate the absorption rate of sulphur dioxide into the droplets of limestone slurry has been developed and implemented into a commercial CFD code. The model has been used to simulate a full-scale FGD unit for which the empirical correlations failed to predict the performances in terms of pressure drop and removal efficiency. The flue gas has been considered already saturated with water at the absorber inlet, thus saving computational time. Three different operating conditions have been simulated by varying the number of the operating spray levels. The calculated value of sulphur dioxide removal efficiency does not vary significantly for the cases with five and four spray levels in operation, with and without droplet rebounds on the walls. The simulation with three levels in operation shows rather different results for the two droplet–wall interaction models. The case with liquid deposition on the walls shows an inhomogeneous distribution of $SO_2$ and values of removal efficiency much lower than the case with ideal reflection of the impacting droplets. The reason is that a substantial fraction of the injected slurry flow rate is lost on the walls contributing only partially to sulphur dioxide removal. This effect is not significant for the cases with five and four operating levels with wall deposition because the slurry flow rate is so high that the liquid fraction deposited on the walls does not influence the resulting $SO_2$ removal efficiency.

The calculated numerical values of pressure drop and $SO_2$ removal efficiency agree well with the experimental data for the different operating conditions. Particularly, the calculated values of $SO_2$ removal efficiency are in very good agreement with measurement.

It can be concluded that the developed model is a powerful tool in the design and optimization of desulphurisation Open Spray Tower equipment, e.g. allowing to evaluate numerically (without the need of a physical model) the best positioning of the spraying nozzles, the distance between the spray levels, the size of the wall rings, the number of operating spray levels and other critical parameters.

The main source of empiricism pertains to the empirical correlations determining the mass transfer coefficients and the $SO_2$ enhancement factor, the latter considered constant. A more realistic model accounting for the variation of it and the desorption of $CO_2$ is currently under development.

## Acknowledgement

The author would like to thank the Department of Energy of the Politecnico di Milano.

## References

[1] J.S. Klingspor, D.R. Cope, FGD Handbook, EA Coal Research, London, 1987.
[2] R.R. Mehta, Modeling of $SO_2$ removal and Limestone Utilization in Slurry Scrubbing Systems with Forced Oxidation, M.S. Thesis, University of Texas, Austin, 1982.
[3] S. Olausson, M. Wallin, I. Bjerle, A model for the absorption of sulfur dioxide into a limestone slurry, Chemical Engineering Journal 51 (1993) 99–108.
[4] R.S. Agarwal, G.T. Rochelle, Chemistry of limestone slurry scrubbing, in: 1993 $SO_2$ Control Symposium, vol. 3, Boston, MA, 1993, p. 78.
[5] C. Brogren, H.T. Karlsson, Modeling the absorption of $SO_2$ in a spray scrubber using the penetration theory, Chemical Engineering Science 52 (18) (1997) 3085–3099.
[6] D. Eden, M. Luckas, A heat and mass transfer model for the simulation of the wet limestone flue gas scrubbing process, Chemical Engineering Technology 21 (1) (1998) 56–60.
[7] S. Kiil, M.L. Michelsen, K. Dam-Johansen, Experimental investigation and modelling of a wet flue gas desulfurization pilot plòant, Industrial and Engineering Chemistry Research 37 (88) (1998) 2792–2806.
[8] J. Warych, M. Szymanowski, Model of the wet limestone flue gas desulfurization process for cost optimization, Industrial and Engineering Chemistry Research 40 (2001) 2597–2605.
[9] H.G. Nygaard, S. Kiil, J.E. Johnson, J. Jensen, J. Hansen, F. Fogh, K. Dam-Johansen, Full-scale measurements of $SO_2$ gas phase concentrations and slurry compositions in a wet flue gas desulphurisation spray absorber, Fuel 83 (9) (2004) 1151–1164.
[10] A. Gomez, N. Fueyo, A. Tomas, Detailed modelling of a flue-gas desulfurisation plant, Computers and Chemical Engineering 31 (2007) 1419–1431.
[11] L. Marocco, F. Inzoli, Multiphase Euler–Lagrange CFD simulation applied to wet flue gas desulphurisation technology, International Journal of Multiphase Flow 35 (2009) 185–194.
[12] A. Lapin, A. Lübbert, Numerical simulation of dynamics of two-phase gas flow in bubble columns, Chemical Engineering Science 49 (1994) 3661–3674.
[13] C.T. Crowe, M. Sommerfeld, Y. Tsuji, Multiphase Flow with Droplet and Particles, CRC Press, Boca Roton, 1998.
[14] T.H. Shih, W.W. Liou, A. Shabbir, Z. Yang, J. Zhu, A new $k$–$\varepsilon$ Eddy-viscosity model for high Reynolds number turbulent flows—model development and validation, Computer Fluids 24 (3) (1995) 227–238.
[15] S.A. Morsi, A.J. Alexander, An investigation of particle trajectories in two-phase flow systems, Journal of Fluid Mechanics 55 (1972) 193–208.
[16] R.H. Perry, D.W. Green, Perry's Chemical Engineers' Handbook, seventh ed., McGraw-Hill, USA, 1998.
[17] G. Maurer, On the solubility of volatile weak electrolytes in aqueous solutions, ACS Symposium Series 133 (1980) 139–172.
[18] C.L. Gage, G.T. Rochelle, Limestone dissolution in flue gas scrubbing: effect of sulfite, Journal of Air Waste Management Association 42 (1992) 926–935.
[19] L.A. Bromley, Approximate individual ion values of β (or B) in extended Debye–Hückel theory for uni-univalent aqueous solutions at 298.15 K, Journal of Chemical Thermodynamics 4 (1972) 669.
[20] L. Marocco, Multiphase Euler–Lagrange CFD study applied to Wet Flue Gas Desulphurisation, PhD thesis, Politecnico di Milano, Milano, Italy, 2008.
[21] C. Weiss, U. Wieltsch, Laser optical flow measurements and computational fluid dynamic calculation of spray tower hydrodynamics, Chemical Engineering Research and Design 83 (2004) 1–17.
[22] ABB FLÄKT, EU Patent No. EP 0963235B1, 1998.
[23] C. Brogren, R. Hakansson, K. Benton, P. Rader, Performance enhancement plates (PEP): up to 20 percent reduction in power consumption of WFGD, in: Combined Power Plant Pollutant Control Mega Symposium, 1999.
[24] J. Hofelsauer, W. Notter, L. Marocco, M. Agalioti, P. Leoussis, Improvement of $SO_2$ removal with application of wall rings and advanced CFD modelling—the case of FGD unit Megalopolis, VGB Power Technology 3 (2008) 85–89.